Acta Oceanol. Sin., 2017, Vol. 36, No. 9, P. 27–38
DOI: 10.1007/s13131-017-1108-x
http://www.hyxb.org.cn
E-mail: hyxbe@263.net

An evaluation of new satellite-derived latent and sensible heat fluxes with moored buoy data, OAFlux and NCEP2 reanalysis products

ZHANG Lei[1]*, SHI Hanqing[1]

[1] Institute of Meteorology and Oceanography, National University of Defense Technology, Nanjing 211101, China

Received 17 March 2016; accepted 23 June 2016

Abstract

New satellite-derived latent and sensible heat fluxes are performed by using WindSat wind speed, WindSat sea surface temperature, the European Centre for Medium-range Weather Forecasting (ECMWF) air humidity, and ECMWF air temperature from 2004 to 2014. The 55 moored buoys are used to validate them by using the 30 min and 25 km collocation window. Furthermore, the objectively analyzed air-sea heat fluxes (OAFlux) products and the National Centers for Environmental Prediction-National Center for Atmospheric Research reanalysis 2 (NCEP2) products are also used for global comparisons. The mean biases of sensible and latent heat fluxes between WindSat flux results and buoy flux data are –0.39 and –8.09 W/m^2, respectively. In addition, the root-mean-square (RMS) errors of the sensible and latent heat fluxes between them are 5.53 and 24.69 W/m^2, respectively. The RMS errors of sensible and latent heat fluxes are observed to gradually increase with an increasing buoy wind speed. The difference shows different characteristics with an increasing sea surface temperature, air humidity, and air temperature. The zonal average latent fluxes have some high regions which are mainly located in the trade wind zones where strong winds carry dry air in January, and the maximum value centers are found in the eastern waters of Japan and on the US east coast. Overall, the seasonal variability is pronounced in the Indian Ocean, the Pacific Ocean, and the Atlantic Ocean. The three sensible and latent heat fluxes have similar latitudinal dependencies; however, some differences are found in some local regions.

Key words: latent and sensible heat fluxes, WindSat, ECMWF reanalysis data, OAFlux

Citation: Zhang Lei, Shi Hanqing. 2017. An evaluation of new satellite-derived latent and sensible heat fluxes with moored buoy data, OAFlux and NCEP2 reanalysis products. Acta Oceanologica Sinica, 36(9): 27–38, doi: 10.1007/s13131-017-1108-x

1 Introduction

The atmosphere and the ocean are closely linked by the transfer of energy (heat and momentum), water, and gases between them. Accurate turbulent air-sea fluxes are of great importance in studying air-sea interaction issues. The turbulent exchange of heat between the atmosphere and the ocean involves latent heat flux and sensible heat flux, which are very useful for global energy research and application.

The latent and sensible heat fluxes can be measured directly. Some experiments have been performed for detecting them (Webster and Lukas, 1992; Fairall et al., 1997; Godfrey et al., 1998; Raschke et al., 2001; Smith et al., 2001). Most direct measurements are difficult and costly, so they are only made on a few research vessels. This in turn limits the time and space of an observation. Some bulk aerodynamic algorithms have been established to estimate the latent and sensible heat fluxes globally using more readily available data such as satellite products. Twelve different bulk aerodynamic algorithms were evaluated comprehensively using direct turbulent flux measurements from 12 ship cruises over the tropical and midlatitude oceans (Brunke et al., 2003). Finally, they selected four relatively good algorithms, one of which is a coupled ocean-atmosphere response experiment (COARE) bulk flux algorithm. The COARE bulk flux algorithm has been evolving over several development phases, and some reliable measurements from ship and buoy are used to improve and validate it (Fairall et al., 1996, 2003; Bradley et al., 2000). The COARE version 3.0, as a state-of-the-art algorithm, has been extensively used to calculate the latent and sensible heat fluxes. This algorithm related turbulent fluxes to some surface meteorological parameters such as wind speed, sea surface temperature (SST), air temperature and humidity. These parameters are always obtained from satellite and reanalysis data.

Satellite observations have a vital role in calculating the latent and sensible heat fluxes, especially for passive microwave satellite data. These satellite products such as wind speed and SST have been used to perform some typical data sets of turbulent air-sea fluxes. The representative data sets include the objectively analyzed air-sea fluxes (OAFlux) (Yu et al., 2008), the hamburg ocean atmosphere parameters and fluxes from satellite data (HOAPS) (Andersson et al., 2010; Andersson et al., 2011), the Japanese ocean flux data sets with use of remote sensing observations (J-OFURO) (Kubota et al., 2002), and the Goddard satellite-based surface turbulent fluxes (GSSTF) (Chou et al., 1997; Chou et al., 2003). The input surface meteorological parameters in the OAFlux are derived from some satellites' measurements and reanalyses data produced by the National Centers for Environmental Prediction (NCEP) and European Centre for Medium-range Weather Forecasts (Yu et al., 2008). Satellite data in the OA-

Foundation item: The National Natural Science Foundation of China under contract No. 41576171.
*Corresponding author, E-mail: zlei_best@hotmail.com

Flux synthesis include the wind speed derived from a special sensor microwave/imager (SSMI) (Wentz, 1997), an advance microwave scanning radiometer for earth observing systems (AMSR-E) (Wentz and Meissner, 2000) and QuikSCAT (Freilich et al., 1994), and the SST produced by the study (Reynolds et al., 2002; Reynolds et al., 2007). In addition, this synthesis also includes near-surface humidity product derived from SSMI column water vapor product. For HOAPS-3.2 flux data sets, all meteorological variables are derived from SSMI passive microwave satellite data except for the SST that is the NODC AVHRR Pathfinder data (Yu et al., 2006).

Except for the air temperature, all surface meteorological parameters are derived from satellite data for J-OFURO. The satellite sources of the wind speed include SSMI, AMSR-E, TRMM, QuikSCAT, and the European Space Agency's scatterometer onboard the earth remote sensing (ERS-1/2). SST and sea surface saturated specific humidity are both derived from the NOAA AVHRR and AMSR-E. In addition, air humidity is derived from SSMI. For GSSTF flux data sets, wind speed and air specific humidity are both derived from SSMI, but the SST and 2 m air temperature are both obtained from the NCEP2. It is noted that the GSSTF3 data sets have first been performed for each available individual SSMI measurements that include F08, F10, F11, F13, F14 and F15. In addition, the combined flux data is also produced by averaging all SSMI satellites' data. These different flux data sets have been widely used and play an important role in studying the seasonal evolution of the SST (Yu et al., 2006), a forcing ocean circulation model (Ayina et al., 2006), and studying some phenomena associated with the EI Niño Southern Oscillation (Mestas-Nuñez et al., 2006), etc.

The turbulent fluxes calculated from the moored buoy data have been used to validate those derived from other sources. The previous study (Sun et al., 2003) validates the turbulent heat fluxes obtained from three analyses including NCEP1, NCEP2, and ECMWF by using the moored buoys located in the Atlantic. They found that a time mean oceanic heat loss is systematically overestimated in all the regions. The overestimation in a latent heat loss ranges from about 14 W/m^2 in the eastern subtropical North Atlantic to about 29 W/m^2 in the tropics to about 30 W/m^2 in the midlatitude coastal areas (Sun et al., 2003). Five satellite-derived latent heat flux products were validated by using 75 moored buoys which consist of 66 TAO buoys, 9 National Data Buoy Center (NDBC) buoys and 4 United Kingdom and France buoys (Bourras, 2006). They found HOAPS-2, J-OFURO, GSSTF-2, and the Bourras-Eymard-Liu (BEL)products had moderate systematic errors with respect to surface data, from –13 to 26 W/m^2, and small biases at midlatitudes (6–8 W/m^2). The buoy measurements as well as six diverse latent heat flux products were used to validate a TMI latent heat flux product over the South China Sea (Zeng et al., 2009). They found that the TMI latent flux and the OAFlux approximately reproduce the time variations of the buoy data. Daily satellite-derived latent heat fluxes over the South China Sea (SCSSLH) were performed by using the tropical rain measuring mission (TRMM) microwave imager (TMI) (Wang et al., 2013). The moored buoys, automatic weather station, and cruise observations were used to establish and validate their latent heat flux data sets. In addition, *in situ* buoy measurements are always used to validate the typical satellite-derived turbulent fluxes (Yu et al., 2008).

The accuracy of the turbulent fluxes is due to the true of the surface meteorological parameters, and different data sets always show some differences. The important input parameters of the wind speed and the SST for the representative satellite-derived turbulent fluxes are always derived from some passive microwave sensors such as SSMI, AMSR-E, and TRMM. WindSat, as the first spaceborne fully polarimetric radiometer, can also produce the ocean surface wind speed and the SST (Gaiser et al., 2004). The previous studies (Zhang et al., 2016a, b) have proved that the accuracy of the WindSat wind speed and SST are satisfied and reliable. The purpose of this study is to produce the latent and sensible heat fluxes using the new data sets which include the WindSat wind speed and SST, and validate the new turbulent fluxes by comparing them to the moored buoy measurements and other resources. The air temperature and humidity are obtained from ECMWF data. The COARE Version 3.0 is used to calculate the latent and sensible heat fluxes.

Our paper is organized as follows. In Section 2 the study data sets and method are described. Section 3 continues a detailed results and discussions. Firstly, the basic environmental parameters are evaluated by the moored buoy measurements. Subsequently, the WindSat calculated fluxes are evaluated by the buoy flux data in detail, including by (1) buoy type, and (2) results versus basic variables which contains the wind speed, the SST, the air humidity, and the air temperature. Finally, the OAFlux and NCEP2 products are used for global comparisons which include the seasonal variations and spatial distributions. The conclusions are given in Section 4.

2 Data sets and method

2.1 *Remote sensing data set*

The wind speed and the SST are derived from WindSat which is a fully polarimetric radiometer and operates in five channels: 6.8, 10.7, 18.7, 23.8, and 37.0 GHz. Because of the fully polarimetric channels (10.7, 18.7, and 37 GHz), it can measure not only an ocean surface wind speed but also wind direction (Gaiser et al., 2004). More detailed information can be found at the NRL WindSat website (www.nrl.navy.mil/WindSat). The WindSat products include the wind speed, the wind direction, the SST, a columnar water vapor, a columnar cloud liquid water, and a rain rate. The daily, 3 day period, weekly, and monthly products can be freely downloaded from the Remote Sensing System's website (www.remss.com). The spatial resolution is 0.25°×0.25°. The daily and monthly products are used in this paper, including the SST and the 10 m surface wind speed at low frequency (WSPD_LF). The time series is from January 2004 to December 2014. Figure 1 shows the WindSat global annual mean wind speed and SST from 2004 to 2014.

2.2 *NWP reanalysis*

The four basic variables, including the wind speed, the SST, the air humidity and temperature, are necessary to calculate the sensible and latent heat fluxes. A satellite sensor can offer ocean surface wind speed and SST; however, it has technical difficulties in retrieving the air humidity and temperature at a few meters above the sea surface (Yu et al., 2008). The air humidity and temperature are obtained from the ECMWF data in this study, which have been used to calculate the sensible and latent heat fluxes by some researchers (Kubota et al., 2002; Jiang et al., 2005; Yu et al., 2008). The time series is from January 2004 to December 2014. In addition, the monthly NCEP2 latent and sensible heat fluxes are used to compare our monthly results and they can be freely downloaded from the website (http://www.cpc.ncep.noaa.gov/).

2.3 *The OAFlux products*

The OAFlux products are calculated from the objectively ana-

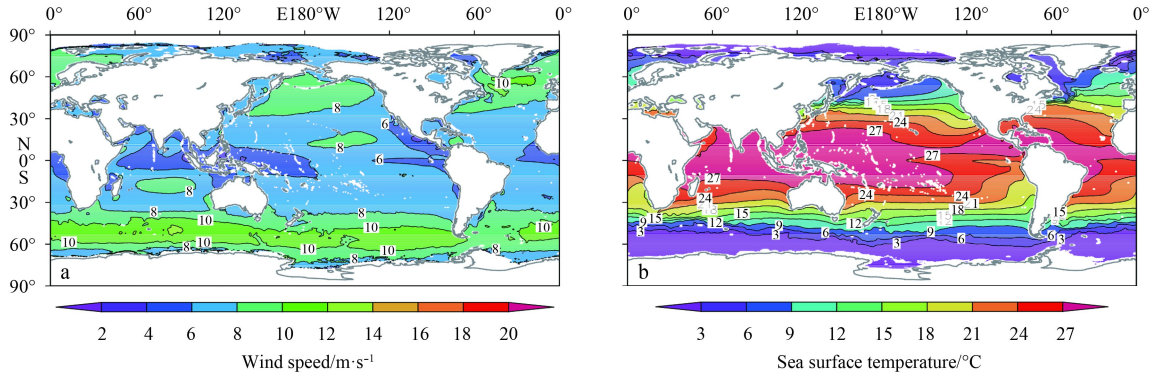

Fig. 1. Time-mean global wind speed (a) and sea surface temperature (b) produced by WindSat monthly products over 11 a from 2004 to 2014. The missing data time includes February 2005 to June 2005, June 2007 to July 2007, and June 2008.

lyzed surface meteorological variables using the COARE bulk flux algorithm 3.0 (Fairall et al., 2003). The computed variables are collected from three major sources which include satellite remote sensing, model reanalyses and ocean surface weather reports from ships. Satellite products in the project include the wind speeds retrieved from QuikSCAT scatterometer and two passive radiometers, and the SST produced by the study (Reynolds et al., 2007). In addition, it also includes a surface humidity product that is produced by using the SSM/I products. The model reanalyses are comprised of two major NWP products which are provided from the NCEP and the ECMWF, respectively. The ship meteorological reports are not assimilated by the OAFlux synthesis because of the sparse coverage. But it is important for identifying biases in NWP model outputs and it was also used to choose the weights for synthesis (Yu et al., 2008). The global time series of the ocean sensible and latent heat fluxes can be obtained from the website (http://oaflux.whoi.edu) [from 1958 to present], which include 1° gridded daily-mean (1985 onward) and monthly-mean (1958 onward) products. The study (Yu et al., 2008) shows that the difference between the OAFlux (sensible and latent heat fluxes) and the buoy is small, about 1.0 W/m^2, and the mean difference in absolute measure is 7.4 W/m^2. In order to compare the WindSat monthly results, the OAFlux monthly products are selected during the periods from January 2004 to December 2014. The annual average monthly products are shown in Fig. 2.

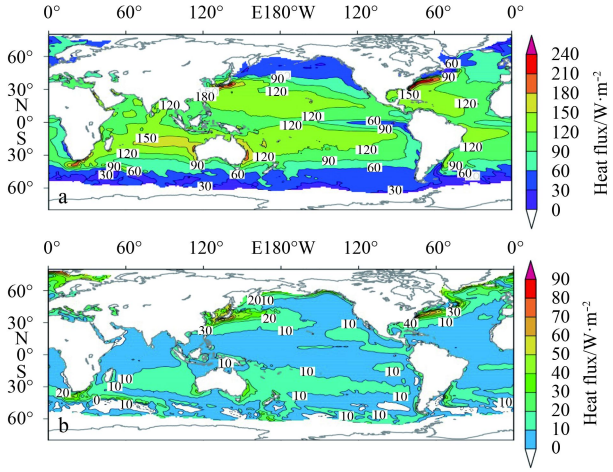

Fig. 2. Time-mean global turbulent fluxes produced by OAFlux monthly products over the 11 complete years from 2004 to 2014. a. Latent heat flux and b. sensible heat flux.

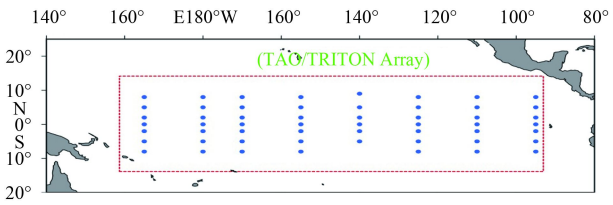

Fig. 3. The distribution of selected buoy.

2.4 *Buoy measurements*

The buoy observations are always used to validate latent and sensible heat fluxes calculated by other resources (such as satellite measurements or the NWP reanalyses) over a long-term period (Yu et al., 2008; Zeng et al., 2009). The selected moored buoys are derived from the tropical atmosphere-ocean/triangle trans-ocean buoy (TAO/TRITON) array, which are located in the tropical Pacific Ocean (McPhaden et al., 1998). The distribution of the selected 55 buoys is shown in Fig. 3. The selected observations of the TAO/TRITON array consist of the wind speed, the SST, the air temperature, and the relative humidity. The wind speed is given at a height of 4 m above mean sea level. The SST is given at a depth of 1 m. The accuracy of the SST measurements from the moored and drifting buoys was evaluated by the study (Castro et al., 2012). The results show that the tropical moored buoys show no significant differences in measurement, and good quality measurements can be found from the moored buoys. The relative humidity and the air temperature are both given at a height of 3 m above the mean sea level. All of the measurements are made at a sample rate of 10 min. The technical details can be found at the website (http://www.pmel.noaa.gov/tao/).

2.5 *Method*

The COARE bulk algorithm has been extensively used to calculate the turbulent heat fluxes, and the latest version is 3.0 (Brunke et al., 2003). In turn, the latent heat flux (Q_{lh}) and the sensible heat flux (Q_{sh}) are expressed as

$$Q_{1h}=\rho_{air}C_eUL_e\left(q_s-q_{air}\right), \quad (1)$$

$$Q_{sh}=\rho_{air}C_hUC_p\left(T_a-\theta\right), \quad (2)$$

where ρ_{air} is the air density; C_e and C_h are the turbulent exchange coefficients for the latent and sensible heat fluxes, respectively; U

is wind speed; L_e is the latent heat of evaporation; C_p is the specific heat capacity of air at the constant pressure; q_s and q_{air} are the surface and near-surface atmospheric specific humidities, respectively; T_a is the air temperature at certain height; and θ is the near-surface air potential temperature. Note that the surface atmospheric specific humidity (q_s) is calculated from the saturation humidity (q_{sat}) for pure water at T_s,

$$q_s = 0.98 q_{sat}(T_s), \tag{3}$$

$$q_{sat} = es \times 622/(p - 0.378 \times es), \tag{4}$$

$$es = 6.112 \times \exp\left(17.502 \times \frac{T_s}{T_s + 241}\right) \times (1.000\ 7 + 3.46 \times 10^{-6} \times p), \tag{5}$$

$$\rho_{air} = p \times 100/[287.1 \times (t_{air} + 273.16) \times (1 + 0.61 \times q_{air})], \tag{6}$$

where es is the saturated vapor pressure; p is the pressure; T_s is the SST; and the factor of 0.98 is used to take into account the reduction in the vapor pressure caused by a typical salinity of 34 (Fairall et al., 1996; Zeng et al., 1998).

3 Results and discussion

3.1 *Basic environmental variables*

3.1.1 *Wind speed and SST*

The turbulent heat fluxes are sensitive to the input meteorological parameters, so it is necessary to evaluate these parameters with the in situ measurements. Figure 4 shows the scatter plots of the wind speed and SST among WindSat, buoy, and ECMWF reanalysis data. The top panel shows the wind speed statistics for the WindSat-buoy-ECMWF triplets. Overall, the WindSat wind speed retrievals and ECMWF winds are both smaller than buoy winds in the selected region (see red rectangle in Fig. 3). The WindSat wind speed retrievals show better agreement with buoy measurements than ECMWF winds. The mean bias is 0.10 m/s and the RMS error is 0.74 m/s between the WindSat and buoy measurements. The bottom panel shows the SST statistics for the WindSat-buoy-ECMWF triplets. The ECMWF SST shows good agreement with the buoy SST, and the mean bias is small, about 0.01°C. The WindSat SST retrievals are smaller than the buoy and ECMWF SST, which is about 0.12°C. The RMS errors for the WindSat-buoy-ECMWF triplets range from 0.13 to 0.23°C. The bias and RMS errors are given in the top of each individual panel, and the color denotes the number of samples.

3.1.2 *Specific humidity and air temperature*

The air humidity and air temperature are also critical for estimation of the latent and sensible heat fluxes. In Fig. 5, we compare the buoy air humidity and temperature with the NWP results which include the NCEP2 and ECMWF data. Note that the buoy measures the air humidity and temperature at a height of 3 m above the mean sea level; however, the NWP results are given at a height of 2 m above the mean sea level. The previous study (Sun et al., 2003) showed that the 2 m height-adjusted buoy res-

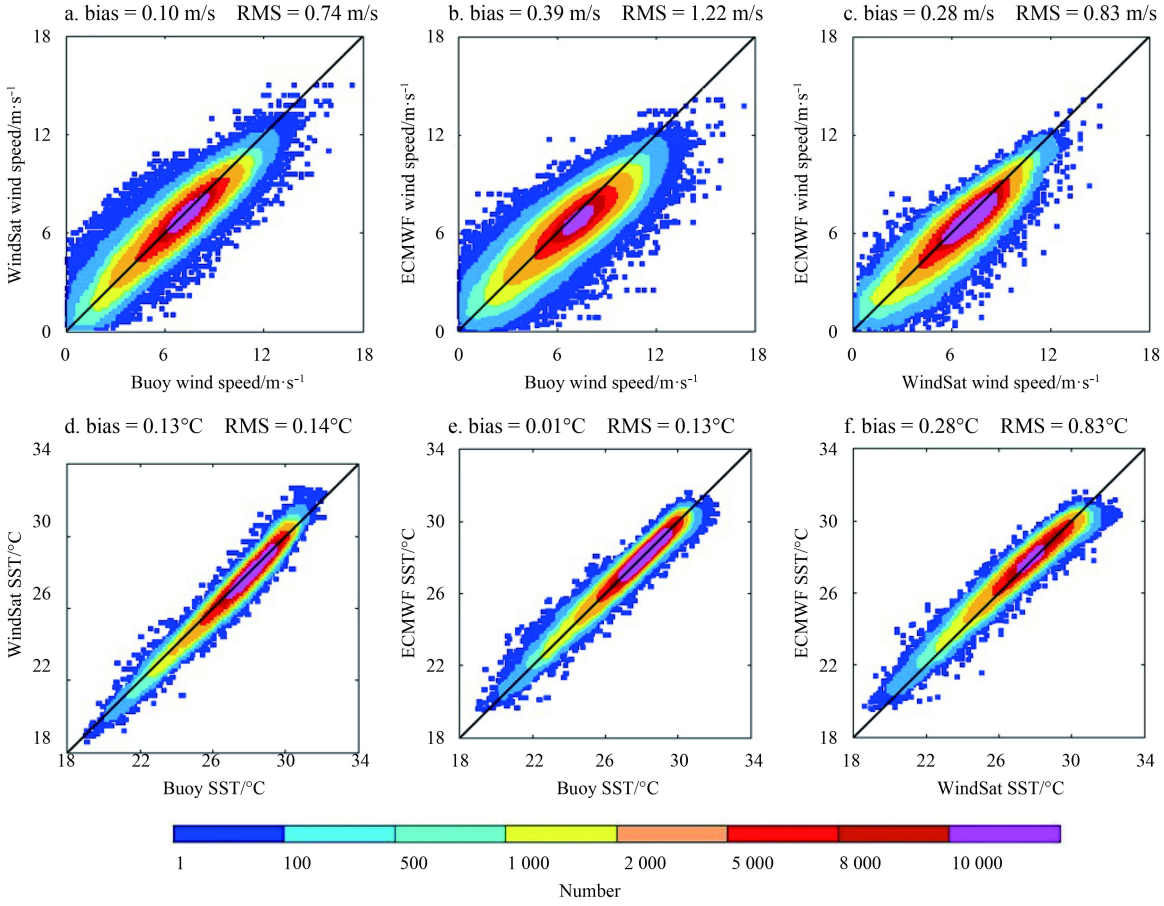

Fig. 4. Intercomparison of the wind speed (the top) and the SST (the bottom) from WindSat, buoy and ECMWF reanalysis data. The bias and the RMS errors are given in the top of each single panel.

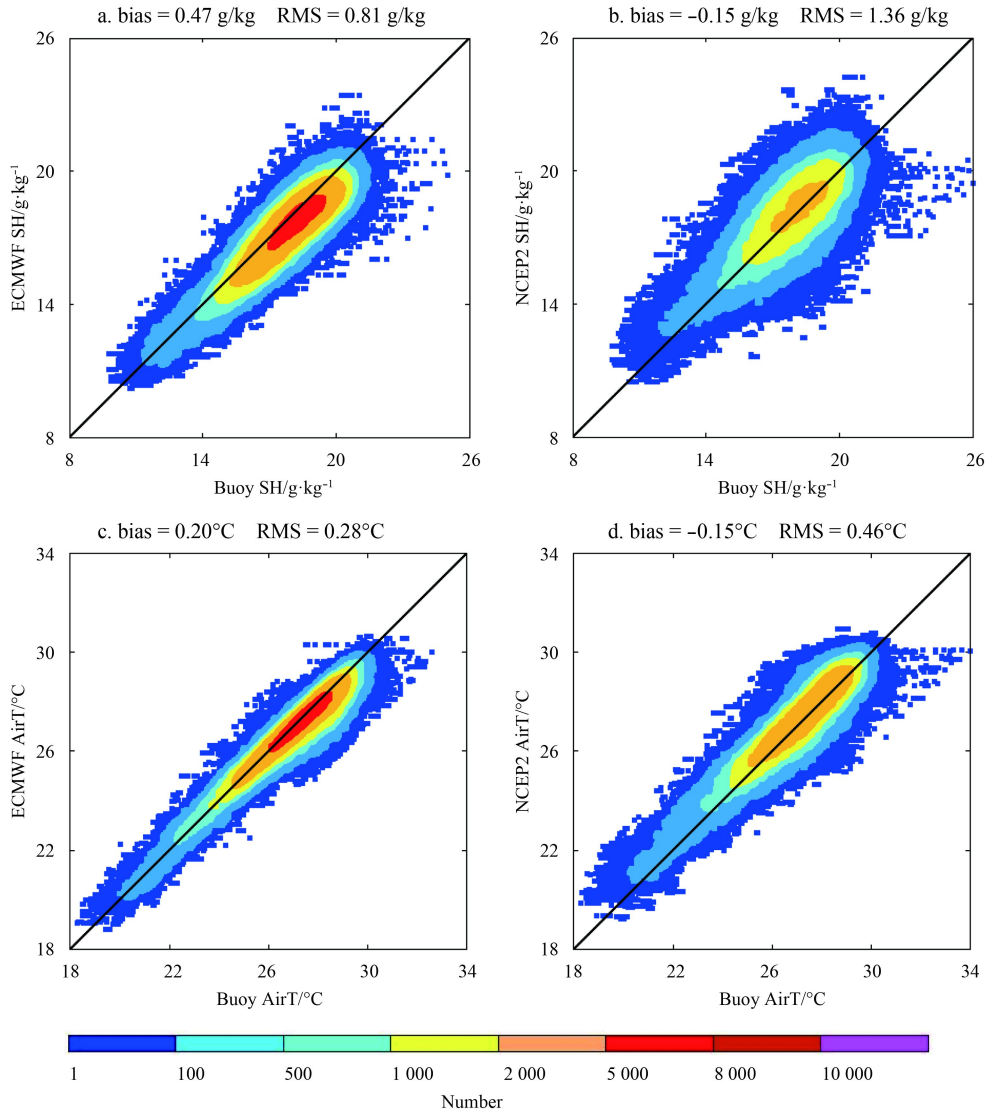

Fig. 5. Comparison of the specific humidity (SH, a and b) and the air temperature (AirT, c and d) between the buoy and NWP (NCEP2 and ECMWF) data. The bias and the RMS errors are given in the top of each panel.

ults were very close in value to the unadjusted ones. So the buoy air humidity and temperature at 3 m are directly used in the comparison. The top panel shows the air humidity statistics between the buoy observations and the NWP data. The buoy measurements are higher than the ECMWF results, and the mean bias is 0.47 g/kg; however, the buoy measurements are smaller than the NCEP2 results, and the mean bias is –0.15 g/kg. The ECMWF air humidity shows better agreement with the buoy observations than the NCEP2 results, and the RMS error is 0.81 g/kg between the ECMWF and buoy data. The bottom panel shows the air temperature statistics between the buoy measurements and the NWP data. The air temperature results are similar to the air humidity results. Compared with the buoy observations, the ECMWF air temperature is relatively small and the NCEP2 air temperature is relatively high.

3.2 *Calculated flux products with moored buoy data*

Based on the WindSat wind speed, the WindSat SST, the ECMWF air temperature, and the ECMWF air humidity, new satellite flux products (hereinafter referred to as WindSat flux products) are produced by using the COARE Version 3.0. In this section, the WindSat flux products are compared with the TAO buoy flux results. For each WindSat flux product, we determine if there is a buoy measurement within 25 km and 30 min of the WindSat calculated result. This results in 316 830 collocations. The comparisons between the WindSat flux products and the TAO buoy fluxes are presented in Fig. 6. The RMS error of the sensible heat flux between the WindSat flux products and the buoy fluxes is 5.53 W/m^2, and that of the latent heat flux between them is 24.69 W/m^2. Overall, the mean biases of the sensible and latent heat fluxes are –0.39 and –8.09 W/m^2, respectively. That means the WindSat flux products tend to be high.

To better characterize the WindSat flux products relative to those from the buoys, the geographic distributions of the above results are shown in Figs 7 and 8, where each square represents one buoy. Figure 7 shows the statistical results of bias about latent and sensible heat fluxes. The top panel shows the statistical result of the latent heat flux. The maximum negative and positive biases only occur for a few selected buoys. For buoys in a band from 5°N to 9°N, the mean bias is negative. The bottom panel shows the result of the sensible heat flux. For buoys in a band from 4°S to 4°N, the WindSat sensible heat fluxes are mainly

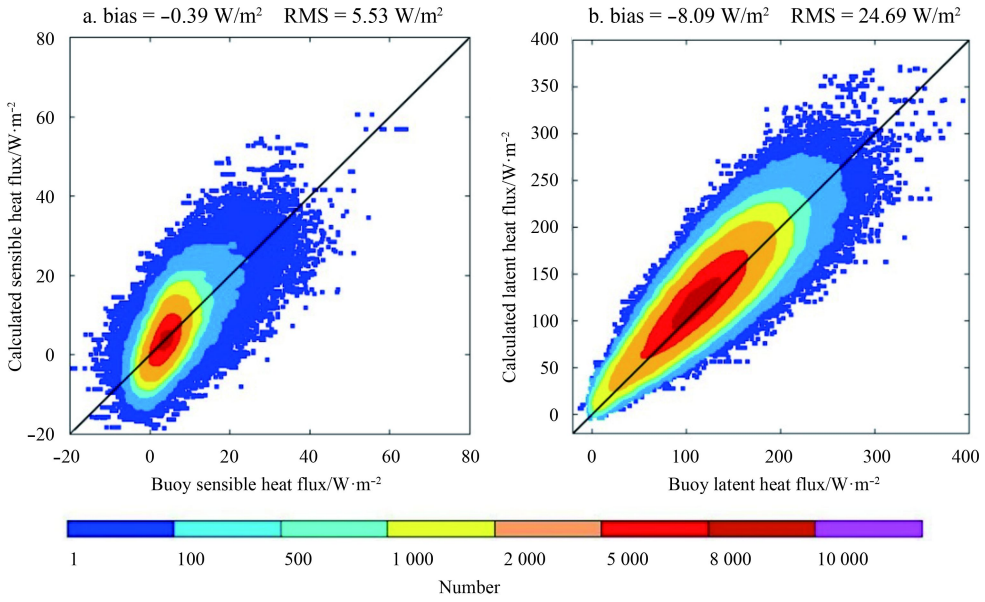

Fig. 6. Turbulent fluxes retrievals from the WindSat and ECMWF reanalysis data versus the buoy results. a. Sensible heat flux, and b. latent heat flux.

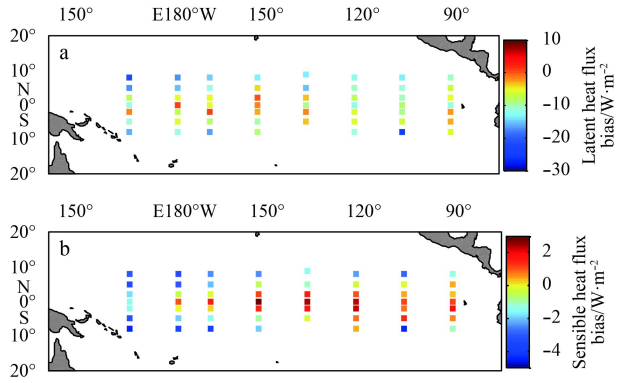

Fig. 7. Maps of the turbulent fluxes bias between the WindSat and buoy results. a. The latent heat flux and b. the sensible heat flux.

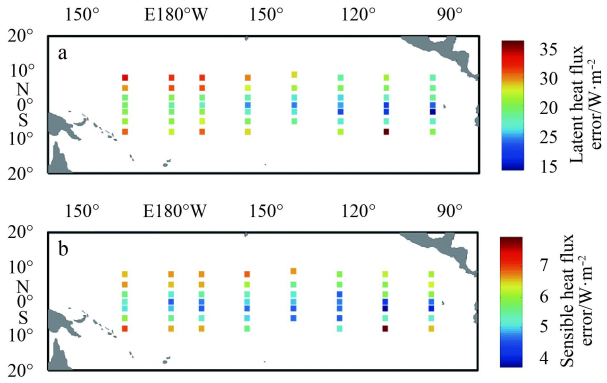

Fig. 8. Maps of the turbulent fluxes RMS errors between the WindSat and buoy results. a. The latent heat flux, average RMS error being 24.69; and b. the sensible heat flux, average RMS error being 5.53.

lower than those calculated by buoys. On the contrary, for buoys located in a range of 5°N to 9°N and over 8°S, the WindSat sensible heat fluxes are mainly higher than those calculated by the buoys. In addition, the WindSat sensible heat fluxes tend to be high near the west Pacific. Figure 8 shows the statistical results of the RMS error about latent and sensible heat fluxes. Overall, the maximum RMS errors are mainly located on either side of the equator, and the RMS errors are relatively small near the equator.

3.3 *Calculated flux products versus basic variables*

In this section, the latent heat flux errors are plotted as a function of input environmental parameters in Fig. 9. Figure 9a shows the difference of the WindSat latent heat flux minus the buoy calculated result plotted versus the buoy wind speed. The mean bias of the latent heat flux is negative when the buoy wind speed is less than 10 m/s. On the contrary, the mean bias becomes positive when the buoy wind speed is more than 10 m/s. The RMS error is observed to gradually increase with increasing wind speed. Figures 9b and c show the difference of the WindSat latent heat flux minus the buoy calculated result plotted versus the buoy SST and the ECMWF air temperature, respectively. Overall, the mean bias and the RMS error are increasing with increasing SST and increasing air temperature. Figure 9d shows the difference of the WindSat latent heat flux minus the buoy calculated result plotted versus the ECMWF air humidity. The mean bias of the latent heat flux becomes negative when the ECMWF specific humidity is more than 13 g/kg. In addition, the mean bias and the RMS error are gradually increasing with the increasing specific humidity.

Figure 10 shows the difference of the WindSat sensible heat flux minus buoy calculated result plotted versus the buoy wind speed, the buoy SST, the ECMWF air temperature, and the ECMWF specific humidity. The RMS error is also observed to gradually increase with the increasing wind speed. The mean bias is positive when the SST is less than 26°C; however, the mean bias becomes negative when the SST is more than 26°C, and the difference is first increasing and then decreasing with the increasing SST. With the increasing air temperature, the performances are similar to the SST results. When the specific humidity is less than 13 g/kg or is more than 17 g/kg, the mean bias is negative.

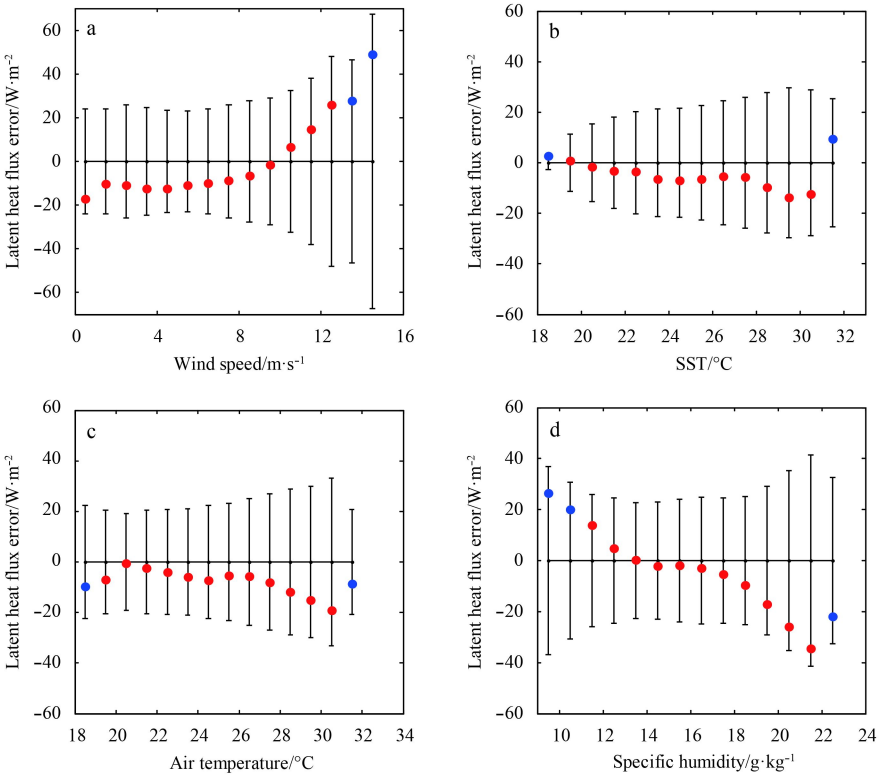

Fig. 9. The latent heat flux errors between the WindSat and buoy retrievals plotted as a function of environmental parameters: wind speed (a), sea surface temperature (b), air temperature (c), and specific humidity (d). The red dots denote that the matching collocations are more than 500, and the blue dots denote that the matching collocations are less than 500.

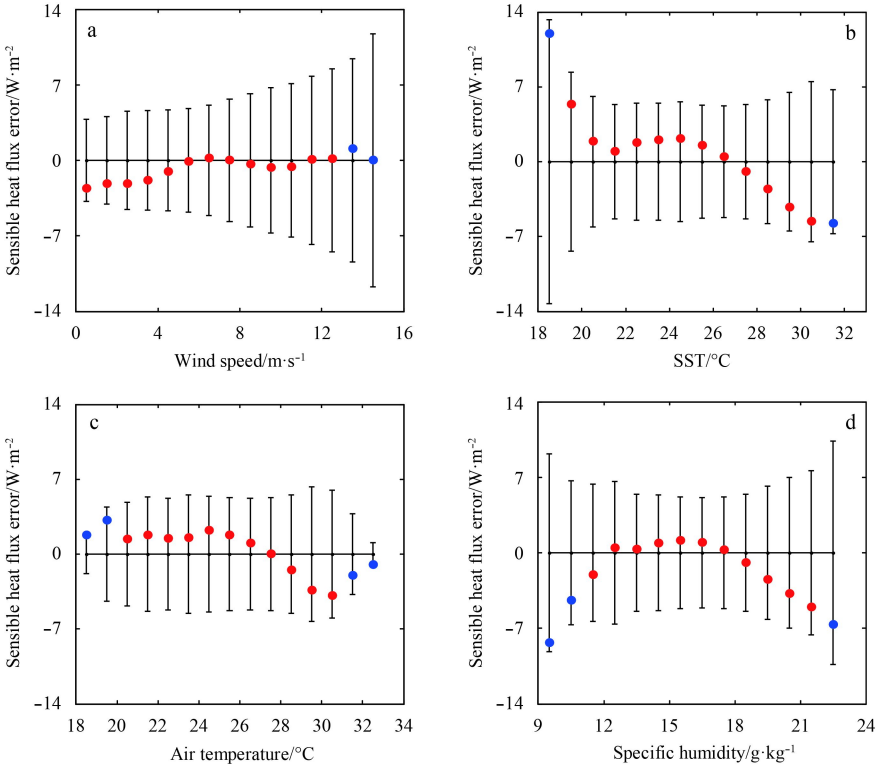

Fig. 10. The sensible heat flux errors between the WindSat and buoy retrievals plotted as a function of environmental parameters: wind speed (a), sea surface temperature (b), air temperature (c), and specific humidity (d). The red dots denote the matching collocations are more than 500.

3.4 *Comparison with OAFlux and NCEP2 data*

The seasonal variations and spatial distributions of the latent and sensible heat fluxes are discussed in this section. The OAFlux and NCEP2 products are selected for global comparisons. The WindSat latent and sensible heat fluxes are computed from the monthly mean values of the WindSat wind speed, the WindSat SST, the ECMWF air temperature, and the ECMWF air humidity.

3.4.1 *Latent heat flux in January*

The three annual monthly mean of the latent heat fluxes for January is shown in Fig. 11. The zonal average latent heat fluxes (>150 W/m^2) have some high regions which are mainly located in the trade wind zones where strong winds carry dry air. The latent heat flux is relatively small in the eastern equator Pacific Ocean because of the cold SST and weak winds. Overall, the geographical distribution of the maximum values (>200 W/m^2) shows good agreement for the three different products, which are mainly located in the eastern waters of Japan and the US east coast. But some differences are found in some local regions. To further summarize the comparisons, the zonally mean fluxes stratified by basins are plotted in Fig. 12. The three latent heat fluxes have similar latitudinal dependencies (Fig. 12). In the Pacific Ocean, the WindSat latent heat flux shows good agreement with the NCEP2 data in a range of 0° to 35°N, and the three latent heat fluxes show good agreement in a range of 35°N to 50°N. In the range 0° to 20°S, the WindSat latent heat flux shows good agreement with the NCEP2 data and they are larger than those from the OAFlux. In the Atlantic Ocean, the results are similar to those in the Pacific Ocean. In the Indian Ocean, the WindSat latent heat flux shows good agreement with the NCEP2 data, and they are a little larger than those from the OAFlux.

3.4.2 *Latent heat flux in July*

The three annual monthly mean of the latent heat fluxes for July is shown in Fig. 13. The seasonal variability is pronounced in the Indian Ocean, the Pacific Ocean, and the Atlantic Ocean. The maximum value centers are mainly located in the Indian Ocean and the eastern waters of Australia (Fig. 14). That is partly associated with the distribution of the strong winds. The lower latent heat fluxes are found at the high latitudes because of the cold SST and the low air humidity. Overall, the three latent heat fluxes have similar latitudinal dependencies in July. At the high latitudes, the WindSat latent heat flux shows good agreement with the OAFlux data. In the range of 35°N to 35°S, the WindSat latent heat flux is always larger than the OAFlux data. The WindSat latent heat flux shows good agreement with the NCEP2 data near the equator.

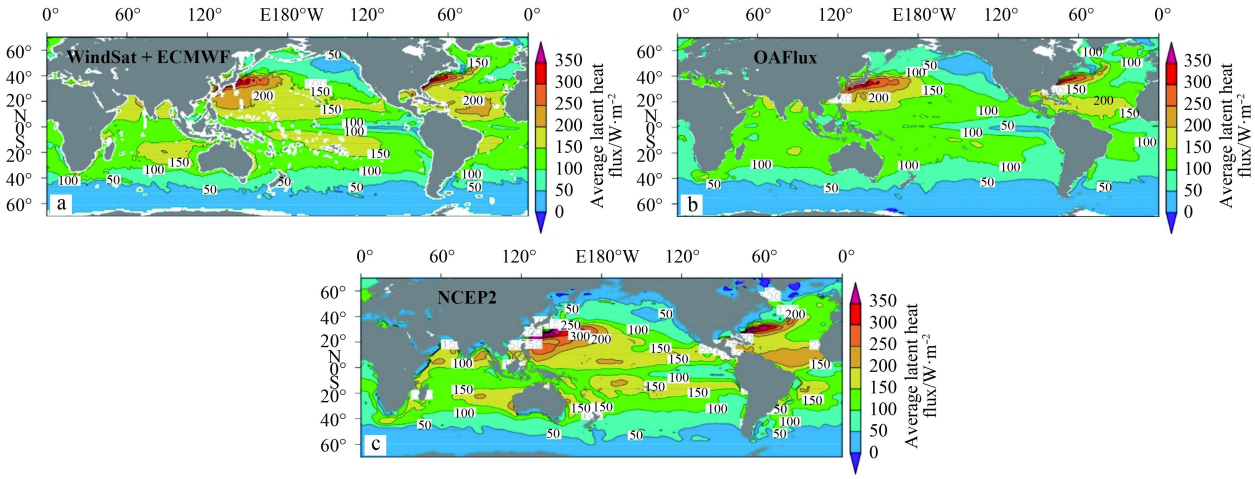

Fig. 11. The latent heat flux in the annual monthly average from 2004 to 2014 for WindSat+ECMWF (a), OAFlux (b), and NCEP2 (c) in January.

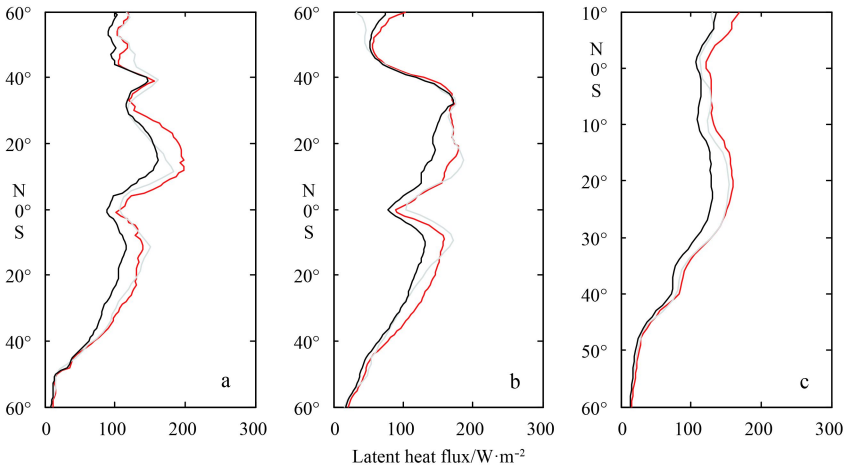

Fig. 12. Latitudinal averages of the WindSat (red color), NCEP2 (grey color), and OAFlux (black color) of the latent heat flux estimated over the Atlantic Ocean (a), the Pacific Ocean (b), and the Indian Ocean (c) in January from 2004 to 2014.

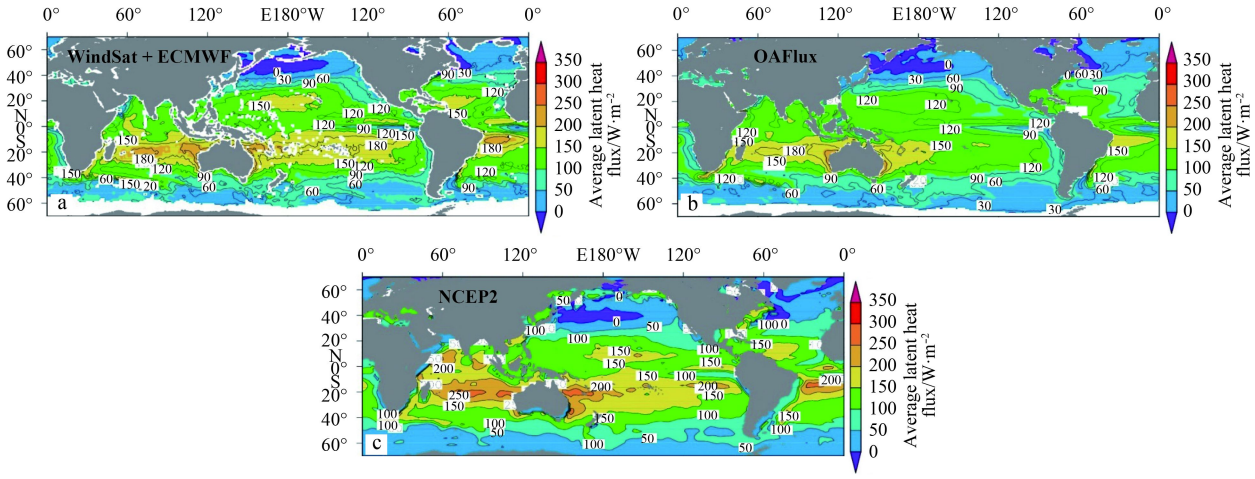

Fig. 13. The latent heat flux in the annual monthly average from 2004 to 2014 for WindSat+ECMWF (a), OAFlux (b), and NCEP2 (c) in July.

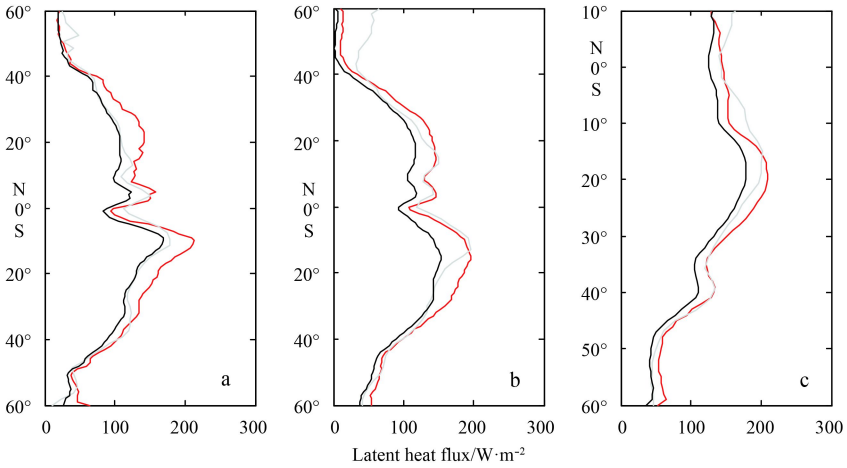

Fig. 14. The latitudinal averages of WindSat (red color), NCEP2 (grey color), and OAFlux (black color) of the latent heat flux estimated over the Atlantic Ocean (a), the Pacific Ocean (b), and the Indian Ocean (c) in July from 2004 to 2014.

3.4.3 *Sensible heat flux in January*

The three annual monthly mean of the sensible heat fluxes for January is shown in Fig. 15. As for the latent heat flux, the sensible heat flux is generally small; however, it cannot be negligible, especially at the high latitudes and over the western boundary current. The sensible heat flux is mainly less than 20 W/m^2 in the tropical region, and increases towards the high latitude of the Northern Hemisphere in January (Fig. 15). The maximum value

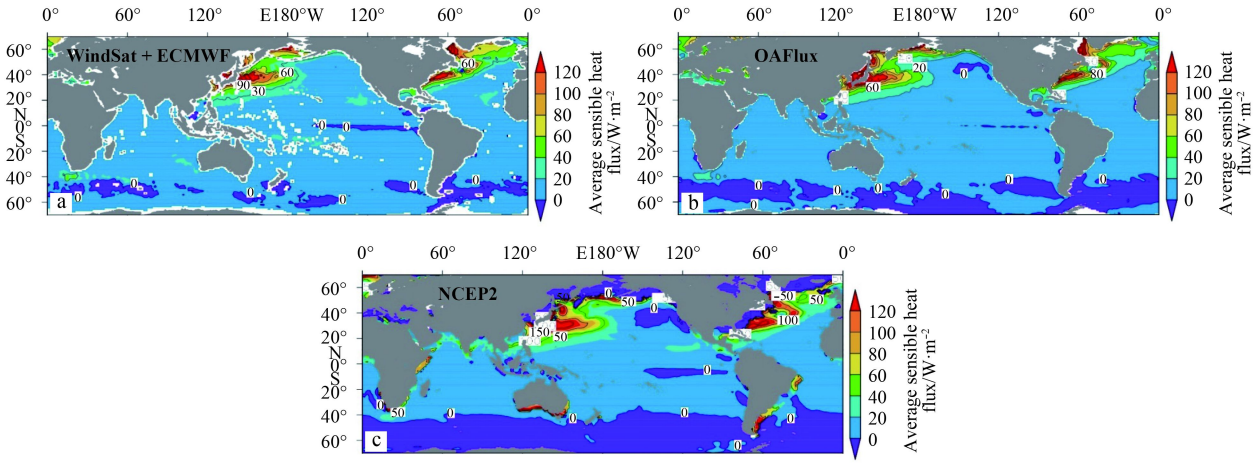

Fig. 15. The sensible heat flux in the annual monthly average from 2004 to 2014 for WindSat+ECMWF (a), OAFlux (b), and NCEP2 (c) in January.

(>80 W/m^2) centers are also located in the eastern waters of Japan and the US east coast. Overall, the WindSat sensible heat fluxes show good agreement with the OAFlux data; however, they have obvious discrepancies with the NCEP2 data at the high latitudes (Fig. 16).

3.4.4 *Sensible heat flux in July*

The three annual monthly mean of the sensible heat fluxes for July is shown in Fig. 17. The seasonal variability is also obvious, and the largest sensible heat loss is located in the Southern Hemisphere. But the strength has diminished in July. In the Northern Hemisphere, the WindSat sensible heat fluxes show good agreement with the OAFlux data (Fig. 18). But in the Southern Hemisphere, the WindSat sensible heat fluxes are almost larger than the OAFlux data. Overall, the three latent heat flux products have also similar latitudinal dependencies.

4 Conclusions

In this study, the new satellite latent and sensible heat fluxes are performed by using the WindSat wind speed, the WindSat SST, the ECMWF humidity, and the ECMWF air temperature from 2004 to 2014. The moored buoy data are used to validate these fluxes with the 30 min and 25 km collocation window. The OAFlux products and NCEP2 products are also used for global comparisons.

The latent and sensible heat fluxes are sensitive to the meteorological parameters, so we firstly compare them with the moored buoy observations. The WindSat wind speed and SST show good agreements with buoy measurements. The mean biases of the wind speed and the SST between them are 0.10 m/s and 0.13°C, respectively. The RMS errors between them are 0.74 m/s and 0.14°C, respectively. Subsequently, we compare the buoy air temperature and humidity with the ECMWF results. The mean bias and RMS error between buoy air temperature and ECMWF result are 0.20°C and 0.28°C, respectively. The ECMWF air temperature shows good agreement with the buoy observation. The ECMWF air humidity is smaller than the buoy data, and the mean bias between them is 0.47 g/kg. The RMS error between them is 0.81 g/kg.

The WindSat and ECMWF products are used to calculate the latent and sensible heat fluxes by using the COARE version 3.0. The moored TAO buoy data are used to validate them. The RMS error of the sensible heat flux between the WindSat flux products and the buoy fluxes is 5.53 W/m^2, and that of the latent heat flux between them is 24.69 W/m^2. The maximum RMS errors are mainly located on either side of the equator, and the RMS errors

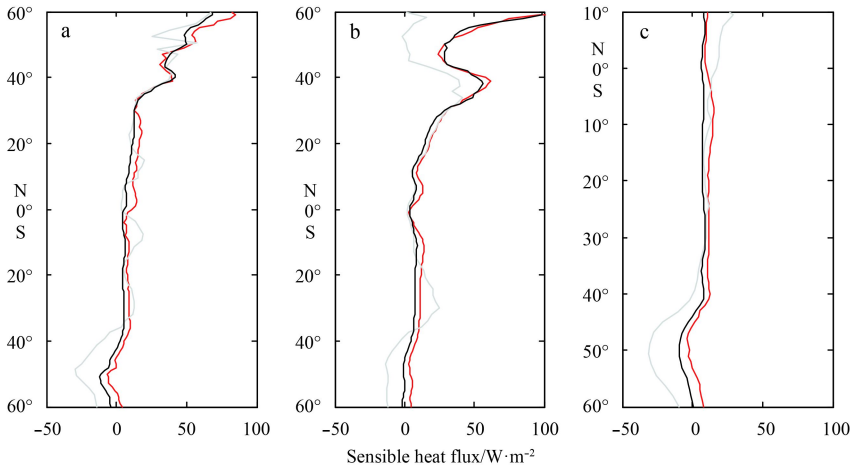

Fig. 16. The latitudinal averages of WindSat (red color), NCEP2 (grey color), and OAFlux (black color) of the sensible heat flux estimated over the Atlantic Ocean (a), the Pacific Ocean (b), and the Indian Ocean (c) in January from 2004 to 2014.

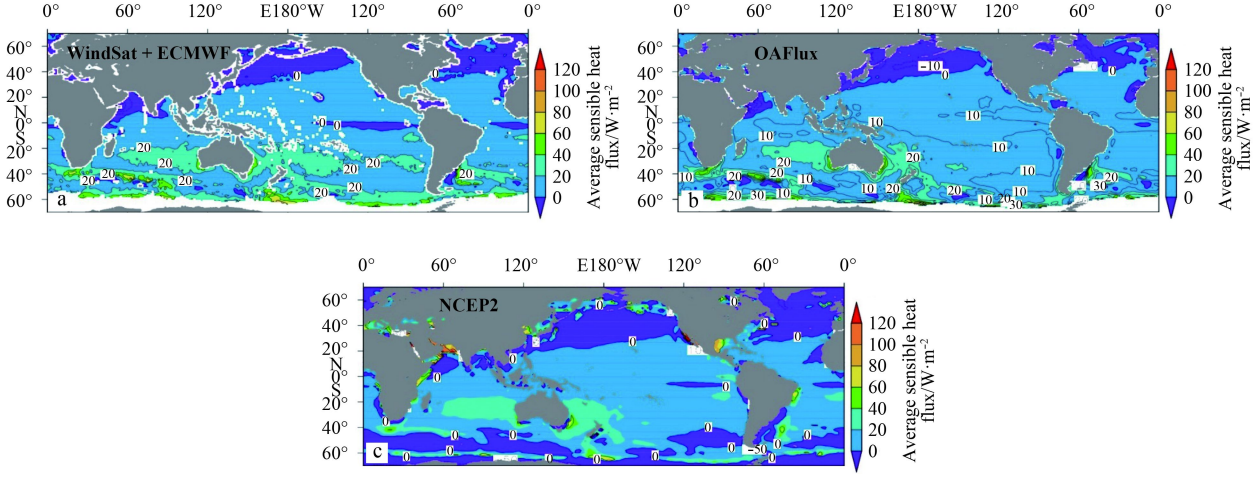

Fig. 17. The sensible heat flux in the annual monthly average from 2004 to 2014 for WindSat+ECMWF (a), OAFlux (b), and NCEP2 (c) in July.

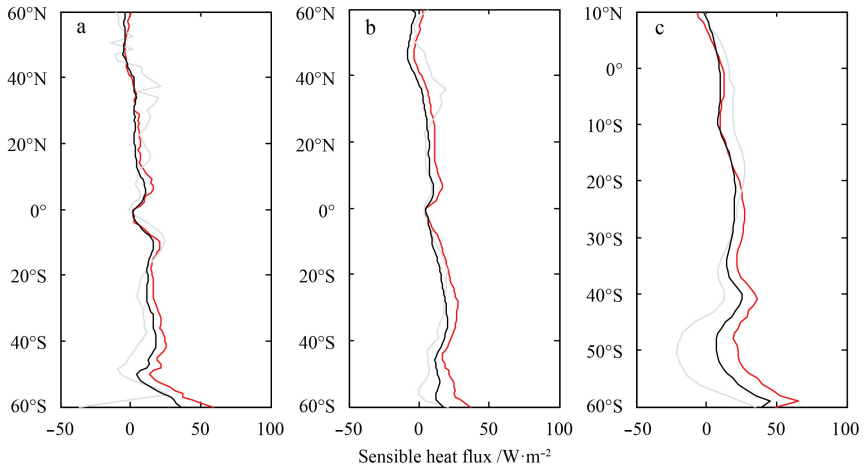

Fig. 18. The latitudinal averages of WindSat (red color), NCEP2 (grey color), and OAFlux (black color) of the sensible heat flux estimated over the Atlantic Ocean (a), the Pacific Ocean (b), and the Indian Ocean (c) in July from 2004 to 2014.

are relatively small in a band from 4°S to 4°N. Overall, the mean biases of the sensible and latent heat fluxes are –0.39 and –8.09 W/m^2, respectively. That means the WindSat flux products tend to be high. The RMS errors of the sensible and latent heat fluxes are observed to gradually increase with the increasing buoy wind speed. Overall, the differences are firstly increasing and then decreasing with the increasing SST and the air temperature.

The seasonal variations and spatial distribution of latent and sensible heat fluxes are discussed by comparing the WindSat heat fluxes with the OAFlux and NCEP2 products. In January, the zonal average latent heat fluxes (>150 W/m^2) have some high regions which are mainly located in the trade wind zones where strong winds carry dry air. The maximum values are mainly located in the eastern waters of Japan and the US east coast. The lower latent heat fluxes are found at the high latitudes because of the cold SST and the low air humidity. In July, the largest value centers are mainly located in the Indian Ocean and the eastern waters of Australia. Overall, the seasonal variability is pronounced in the Indian Ocean, the Pacific Ocean, and the Atlantic Ocean. Generally, the three sensible and latent heat fluxes have similar latitudinal dependencies; however, some differences are found in some local regions.

Compared with the latent heat flux, the sensible heat flux is generally small; however, it cannot be negligible, especially at the high latitudes and over the western boundary current. In January, the largest value (>80 W/m^2) centers are also located in the eastern waters of Japan and the US east coast. Overall, the WindSat sensible heat fluxes show good agreement with the OAFlux data; however, they have obvious discrepancies with the NCEP2 data at the high latitudes. In July, the largest sensible heat loss is located in the Southern Hemisphere. But the strength has diminished. Overall, the three latent heat flux products have also similar latitudinal dependencies.

As for the WindSat, it can retrieve not only the wind speed but also the SST, which can contribute to the calculation of the turbulent fluxes with an ideal time and space resolution. Recently, it has been difficult to evaluate or select the best flux products because of the coarse distribution of buoy and the used different data sources. We hope that this paper may be a good supplement to study the turbulent fluxes.

Acknowledgements

The authors thank C Fairall for providing the COARE flux algorithm 3.0 (http://coaps.fsu.edu/COARE/). They also thank the Remote Sensing Systems for providing WindSat and TMI data (www.remss.com), the Woods Hole Oceanographic Institution for providing the OAFlux (http://oaflux.whoi.edu), the ECMWF data server for providing the ECMWF reanalysis (http://apps.ecmwf.int/datasets/), and the Climate Diagnostics Center for providing the NCEP2 reanalysis (www.esrl.noaa.gov/psd).

References

Andersson A, Fennig K, Klepp C, et al. 2010. The Hamburg ocean atmosphere parameters and fluxes from satellite data-HOAPS-3. Earth Syst Sci Data, 2(2): 215–234

Andersson A, Klepp C, Fennig K, et al. 2011. Evaluation of HOAPS-3 ocean surface freshwater flux components. J Appl Meteor Climatol, 50(2): 379–398

Ayina L H, Bentamy A, Mestas-Nuñez A M, et al. 2006. The impact of satellite winds and latent heat fluxes in a numerical simulation of the tropical Pacific Ocean. J Climate, 19(22): 5889–5902

Bourras D. 2006. Comparison of five satellite-derived latent heat flux products to moored buoy data. J Climate, 19(24): 6291–6313

Bradley E F, Fairall C W, Hare J E, et al. 2000. An old and improved bulk algorithm for air-sea fluxes: COARE2.6a. In: AMS 14th Symposium on Boundary Layer and Turbulence. Aspen, CO: Amer Meteor Soc, 294–296

Brunke M A, Fairall C W, Zeng Xubin, et al. 2003. Which bulk aerodynamic algorithms are least problematic in computing ocean surface turbulent fluxes?. J Climate, 16(4): 619–635

Castro S L, Wick G A, Emery W J. 2012. Evaluation of the relative performance of sea surface temperature measurements from different types of drifting and moored buoys using satellite-derived reference products. J Geophys Res, 117(C2): doi: 10.1029/2011JC007472

Chou S H, Nelkin E, Ardizzone J, et al. 2003. Surface turbulent heat and momentum fluxes over global oceans based on the Goddard satellite retrievals, version 2 (GSSTF2). J Climate, 16(20): 3256–3273

Chou S H, Shie C L, Atlas R M, et al. 1997. Air-sea fluxes retrieved from special sensor microwave imager data. J Geophys Res, 102(C6): 12706–12726

Fairall C W, Bradley E F, Hare J E, et al. 2003. Bulk parameterization of air-sea fluxes: updates and verification for the COARE algorithm. J Climate, 16(4): 571–591

Fairall C W, Bradley E F, Rogers D P, et al. 1996. Bulk parameterization of air-sea fluxes for tropical ocean-global atmosphere coupled-ocean atmosphere response experiment. J Geophys Res, 101(C2): 3747–3764

Fairall C W, White A B, Edson J B, et al. 1997. Integrated shipboard

measurements of the marine boundary layer. J Atmos Oceanic Technol, 14(3): 338–359

Freilich M H, Long D G, Spencer M W. 1994. SeaWinds: A scanning scatterometer for ADEOS II-Science overview. Proc Int Geosci Remote Sens Symp, Vol II. Pasadena, CA: IEEE, No. 94CH3378-7, 960–963

Gaiser P W, St Germain K M, Twarog E M, et al. 2004. The WindSat spaceborne polarimetric microwave radiometer: sensor description and early orbit performance. IEEE Trans Geosci Remote Sens, 42(11): 2347–2361

Godfrey J S, Houze R A Jr, Johnson R H, et al. 1998. Coupled ocean-atmosphere response experiment (COARE): an interim report. J Geophys Res, 103(C7): 14395–14450

Jiang Chuanli, Cronin M F, Kelly K A, et al. 2005. Evaluation of a hybrid satellite- and NWP-based turbulent heat flux product using tropical Atmosphere-Ocean (TAO) buoys. J Geophys Res, 110(C9): doi: 10.1029/2004JC002824

Kubota M, Iwasaka N, Kizu S, et al. 2002. Japanese ocean flux data sets with use of remote sensing observations (J-OFURO). J Oceanogr, 58(1): 213–225

McPhaden M J, Busalacchi A J, Cheney R, et al. 1998. The tropical ocean-global atmosphere observing system: a decade of progress. J Geophys Res, 103(C7): 14169–14240

Mestas-Nuñez A M, Bentamy A, Katsaros K B. 2006. Seasonal and El Niño variability in weekly satellite evaporation over the global ocean during 1996-98. J Climate, 19(10): 2025–2035

Raschke E, Meywerk J, Warrach K, et al. 2001. The Baltic Sea experiment (BALTEX): a European contribution to the investigation of the energy and water cycle over a large drainage basin. Bull Amer Meteor Soc, 82(11): 2389–2413

Reynolds R W, Rayner N A, Smith T M, et al. 2002. An improved in situ and satellite SST analysis for climate. J Climate, 15(13): 1609–1625

Reynolds R W, Smith T M, Liu Chunying, et al. 2007. Daily high-resolution-blended analyses for sea surface temperature. J Climate, 20(22): 5473–5496

Smith S R, Legler D M, Verzone K V. 2001. Quantifying uncertainties in NCEP reanalyses using high-quality research vessel observations. J Climate, 14(20): 4062–4072

Sun Bomin, Yu Lisan, Weller R A. 2003. Comparisons of surface meteorology and turbulent heat fluxes over the Atlantic: NWP model analyses versus moored buoy observations. J Climate, 16(4): 679–695

Wang Dongxiao, Zeng Lili, Li Xixi, et al. 2013. Validation of satellite-derived daily latent heat flux over the South China Sea, compared with observations and five products. J Atmos Oceanic Technol, 30(8): 1820–1832

Webster P J, Lukas R. 1992. TOGA COARE: the coupled ocean-atmosphere response experiment. Bull Amer Meteor Soc, 73(9): 1377–1416

Wentz F J. 1997. A well-calibrated ocean algorithm for special sensor microwave/imager. J Geophys Res, 102(C4): 8703–8718

Wentz F J, Meissner T. 2000. Algorithm theoretical basis document (ATBD) version 2 AMSR ocean algorithm. Remote Sensing Systems Technical Report RSS 121599A.

Yu Lisan, Jin Xiangze, Weller R A. 2006. Role of net surface heat flux in seasonal variations of sea surface temperature in the tropical Atlantic Ocean. J Climate, 19(23): 6153–6169

Yu Lisan, Jin Xiangze, Weller R A. 2008. Multidecade global flux datasets from the objectively analyzed air-sea fluxes (OAFlux) project: latent and sensible heat fluxes, ocean evaporation, and related surface meteorological variables. OAFlux Project Tech Rep OA-2008-01.

Zhang Lei, Shi Hanqing, Du Huadong, et al. 2016a. Comparison of WindSat and buoy-measured ocean products from 2004 to 2013. Acta Oceanologica Sinica, 35(1): 67–78

Zhang Lei, Shi Hanqing, Yu Hong, et al. 2016b. WindSat satellite comparisons with nearshore buoy wind data near the U.S. west and east coasts. Acta Oceanologica Sinica, 35(7): 50–58

Zeng Lili, Shi Ping, Liu W T, et al. 2009. Evaluation of a satellite-derived latent heat flux product in the South China Sea: a comparison with moored buoy data and various products. Atmos Res, 94(1): 91–105

Zeng Xubin, Zhao Ming, Dickinson R E. 1998. Intercomparison of bulk aerodynamic algorithms for the computation of sea surface fluxes using TOGA COARE and TAO data. J Climate, 11(10): 2628–2644